Supplemental information

Self-charging aqueous hydrogen gas batteries

Zhengxin Zhu, Zehui Xie, Weiping Wang, Zaichun Liu, Mingming Wang, Yahan Meng, Qia Peng, Shuang Liu, Taoli Jiang, Kai Zhang, Hongxu Liu, Yirui Ma, Wei Chen*

Department of Applied Chemistry, School of Chemistry and Materials Science, Hefei National Research Center for Physical Sciences at the Microscale, University of Science and Technology of China, Hefei, Anhui 230026, China

*Corresponding author. E-mail address: weichen1@ustc.edu.cn (W. Chen)

Materials.

Pt/C powder (20% Pt on Vulcan XC-72) was purchased from Premetek. Gas diffusion layer (GDL, W1S1009) was purchased from Fuel Cell Store. Activated carbon (AC, YEC-8) was purchased from Fuzhou Yihuan Carbon., Ltd. Glass-fiber separator (GFD, 675 μm) was purchased from Whatman. Polyvinylidene fluoride (PVDF), acetylene black (AB), titanium foil (thickness of 50 μm, 99.99%), and lead foil (thickness of 100 μm, 99.99%) were purchased from MTI. N-methyl-2-pyrrolidone (NMP), H_3PO_4 (85%), NaH_2PO_4, KI, H_2SO_4 (98%), $NiSO_4$, and $K_3Fe(CN)_6$ were purchased from Sinopharm Chemical Reagent Co., Ltd. The electrolyte was prepared using deionized water (resistance of 18.2 MΩ, Milli Q).

Preparation of nickel hexacyanoferrate (NiHCF) materials.

NiHCF was synthesized based on a precipitation reaction in an aqueous solution, according to the previous report.[1] Specifically, 50 mL of 0.2 M $NiSO_4 \cdot 6H_2O$ was dropwisely added into 50 mL of 0.1 M $K_3Fe(CN)_6$ under constant stirring at 70 ℃ for 4 h. After reaction, the precipitates were washed and centrifuged through centrifugation (TG16-WS, Cence Xiangyi) with deionized water and ethanol for three times and then dried in an oven at 65 ℃ for 20 h.

Preparation of PbO_2 electrodes.

A lead foil (6 cm^2) was immersed in 4.5 M H_2SO_4 and galvanostatically charge/discharge cycled in a three-electrode system where the platinum foil and Ag/AgCl electrode were used as the counter and reference electrode, respectively. The current, charging time, discharge cut-off voltage, and cycling time were respectively fixed at 60 mA, 200 s, 1.3 V, and 24 h, which could anodize the surface Pb into PbO_2.

Electrochemical measurements.

The two-electrode tests were performed in Swagelok cells with various cathode materials (AC,

NiHCF, or PbO_2) and Pt/C-catalyzed H_2 anode.[2-4] In the Swagelok cell, the stainless-steel inlet and outlet valves as gas filling channel are connected with Klein Flange adapters (KF25). The anode and cathode are sandwiched by a GFD separator in a plane-parallel electrode geometry, which is tightly placed on between two adapters by a clamp where a polytetrafluoroethylene-centered O-ring as gas sealed component is placed. The three-electrode tests were performed in a beaker cell using PbO_2 working electrode, platinum foil counter electrode and Ag/AgCl reference electrode. AC was mixed with AB and PVDF in a mass ratio of 8:1:1 with the aid of NMP. After being fully ground, the mixture was coated on a titanium foil and dried at 70 ℃ for 12 h under vacuum. The mass loading of AC on the electrode was ~2.5 mg cm^{-2}. Similarly, the PBA cathode was prepared by mixing the NiHCF, AB, and PVDF in a mass ratio of 7:2:1 in NMP. Then, the slurry was coated on a titanium foil and dried at 70 ℃ for 12 h under vacuum. The mass loading of NiHCF on the electrode was ~2 mg cm^{-2}. The electrocatalytic H_2 electrode was made by mixing Pt/C and PVDF with a mass ratio of 9:1 in NMP. The mass loading of Pt/C catalyst on GDL was ~0.2 mg cm^{-2}. CV curves were obtained by a VMP-3 multichannel workstation (Bio-Logic Science Instruments). Galvanostatic charge/discharge curves and cycle performance were measured using Landhe battery test system (CT2001A, Wuhan, China) and Neware battery test system (CT-4008T-5V50mA-164, Shenzhen, China). For the chemically self-charging cells, O_2 was dissolved into the electrolyte and reacted with the discharged cathodes to achieve the self-charging process. For the short-circuit induced self-charging cells and the low-energy-input triggered quasi-self-charging cells, electrochemical ORR reactions took place on the Pt/C electrodes to achieve the self-charging process of the cathodes. For the I_2-H_2 batteries, the electrolyte was 40 μL of 2 M H_3PO_4 and 0.5 M KI. For the PBA-H_2 batteries, the electrolyte was 75 μL of 1 M NaH_2PO_4 and 1 M H_3PO_4 (pH = 1.5) or 1 M NaH_2PO_4 and 0.01 M H_3PO_4 (pH = 3.5). For the PBA-H_2 batteries, the electrolyte was 75 μL of 4.5 M H_2SO_4. In the test experiments, the O_2 is

charged into the Swagelok cell and meanwhile the H_2 is fully eliminated during the self-charging process. Similarly, the H_2 is charged into the Swagelok cell and meanwhile the O_2 is fully eliminated during the subsequent discharge process. The high-purity H_2 and O_2 are respectively sealed in the Swagelok cell during the discharge and self-charging process. Before testing the self-charging performance, the SCAHGBs were firstly activated by five power charge/discharge cycles.

Physicochemical Characterizations.

X-ray diffraction (XRD) patterns were measured by Philips X'Pert PRO SUPER X-ray diffractometer with graphite monochromatized Cu K_α radiation. The morphology was observed from the scanning electron microscopy (SEM, Hitachi8220) equipped with an energy-dispersive X-ray spectrometer to investigate the surface elemental compositions of the materials. Transmission electron microscopy (TEM) image was obtained through the Hitachi-7700 instrument. X-ray photoelectron spectroscopy (XPS) measurements of NiHCF cathode were performed on ESCALAB 250Xi. Raman spectra were collected by Raman spectrometer (InVia Reflex, Renishaw) using a laser with a wavelength of 532 nm.

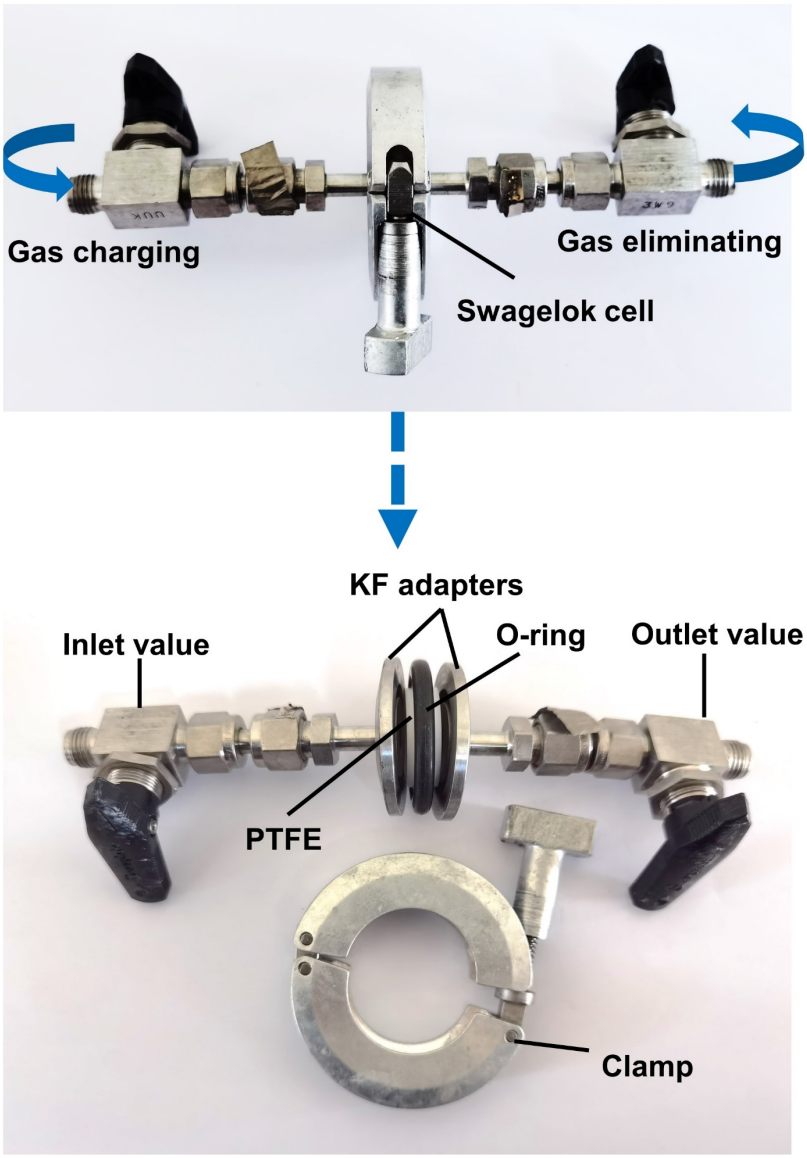

Figure S1. The setup of the self-charging aqueous H_2 cells.

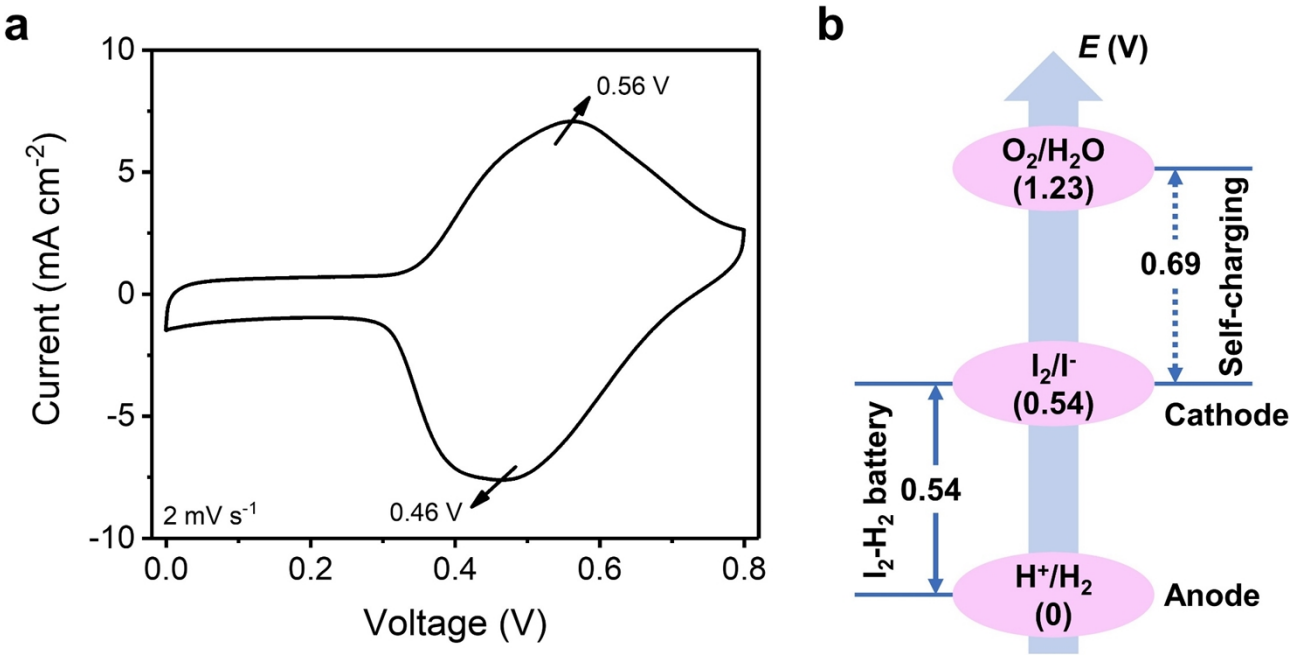

Figure S2. (a) A CV curve of I_2-H_2 battery at a scan rate of 2 mV s^{-1}. (b) Schematic diagram of different electrode potentials of the chemically self-charging I_2-H_2 battery.

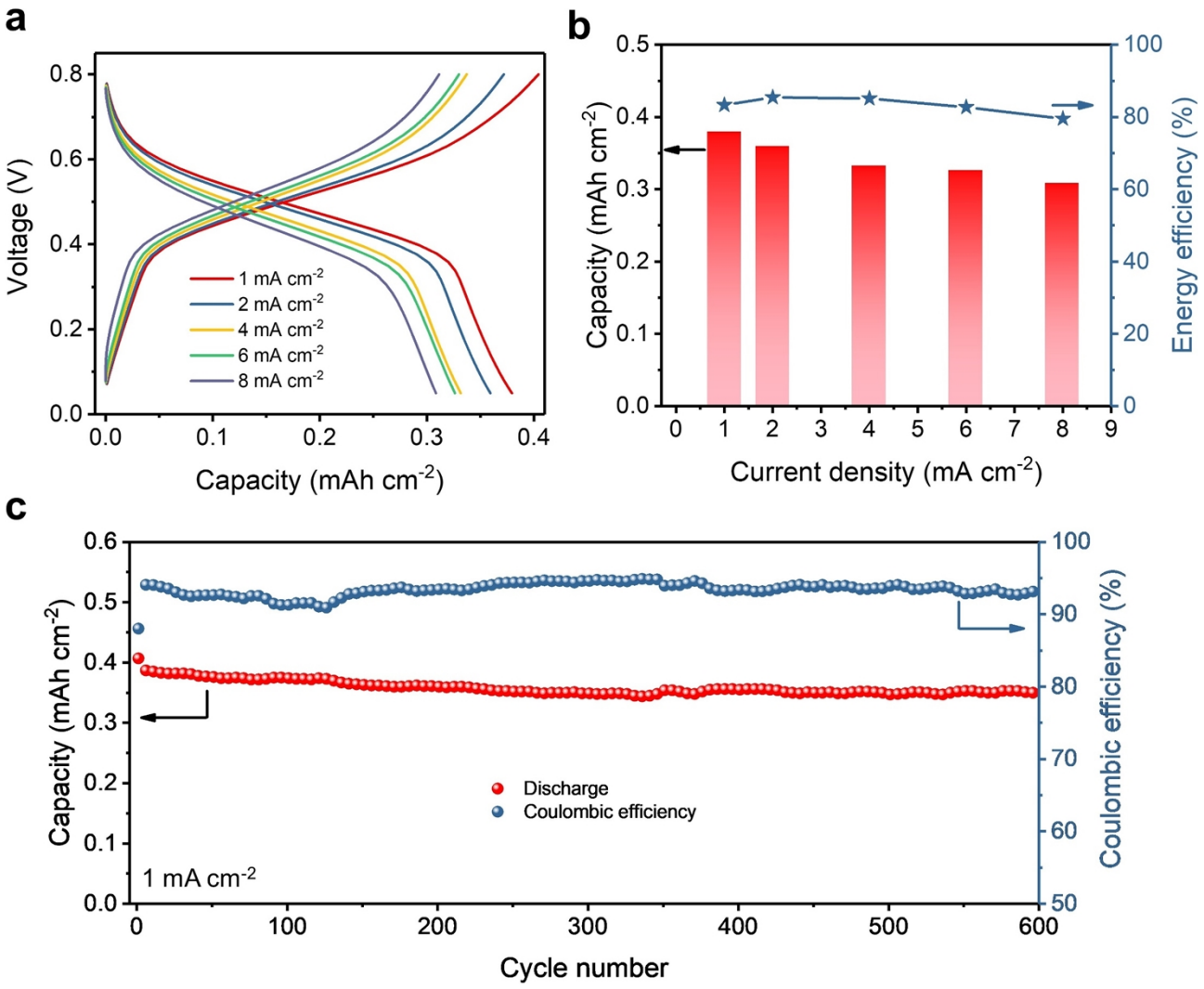

Figure S3. Electrochemical performance of I_2-H_2 batteries. (a) Rate charge/discharge curves. (b) Discharge capacity and energy efficiency at various current densities. (c) Cycle performance at a current density of 1 mA cm^{-2}.

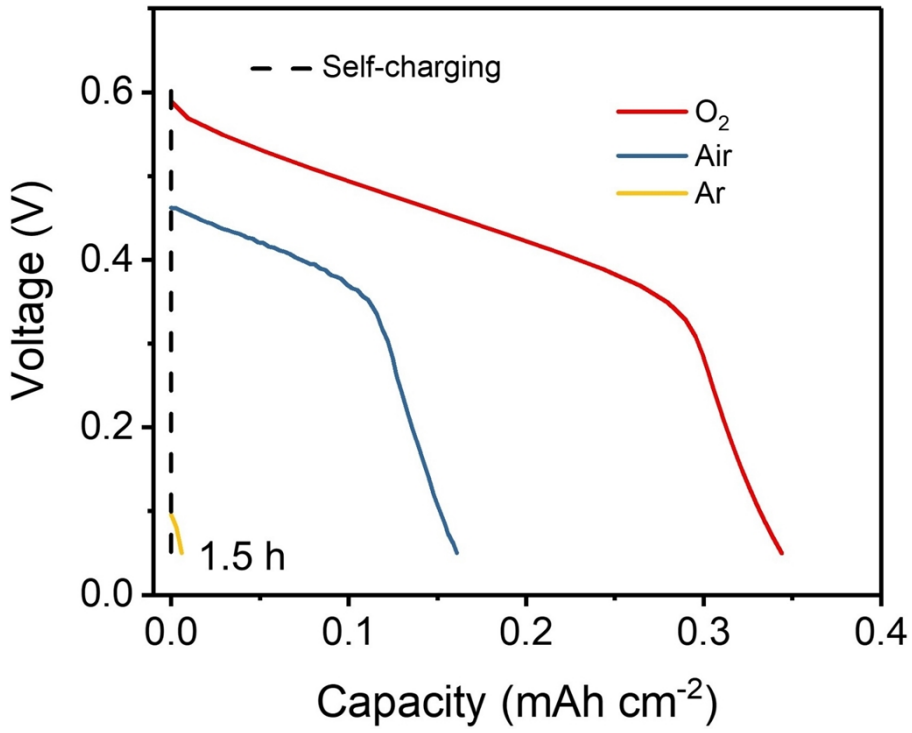

Figure S4. Discharge curves of chemically self-charging I_2-H_2 batteries at a current density of 1 mA cm^{-2} after self-charging in different gas atmospheres for 1.5 h.

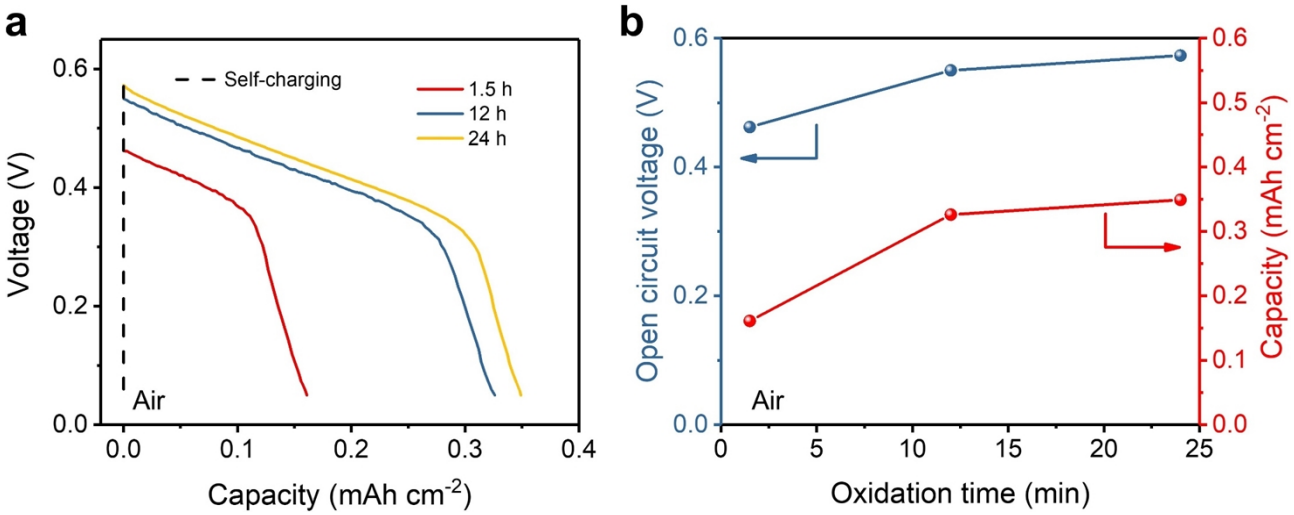

Figure S5. (a) Galvanostatic discharge curves of the chemically self-charging I_2-H_2 batteries at a current density of 1 mA cm^{-2} with different self-charging times by air. (b) Effect of the self-charging time on OCV and discharge capacity.

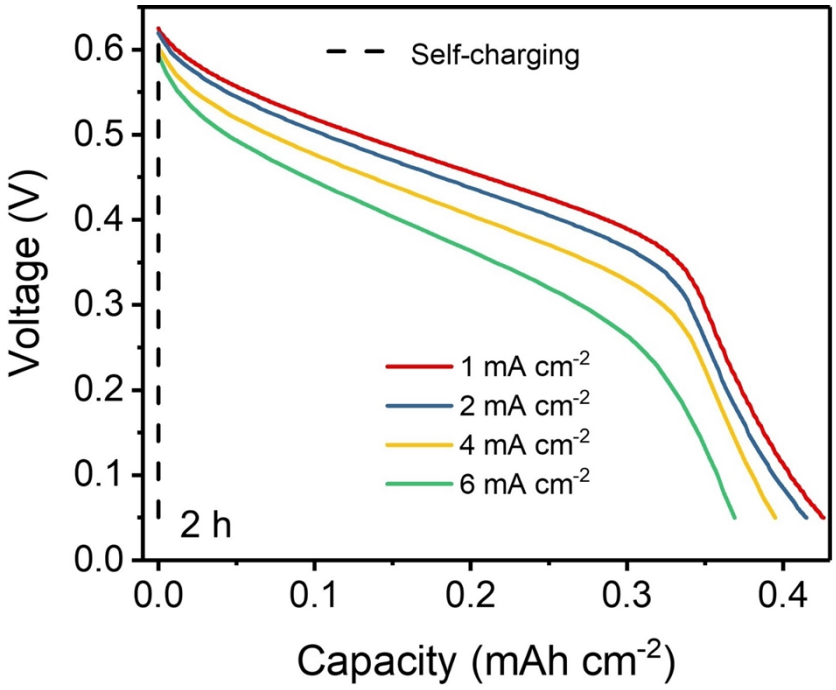

Figure S6. Rate discharge curves of the chemically self-charging I_2-H_2 batteries after self-charging for 2 h.

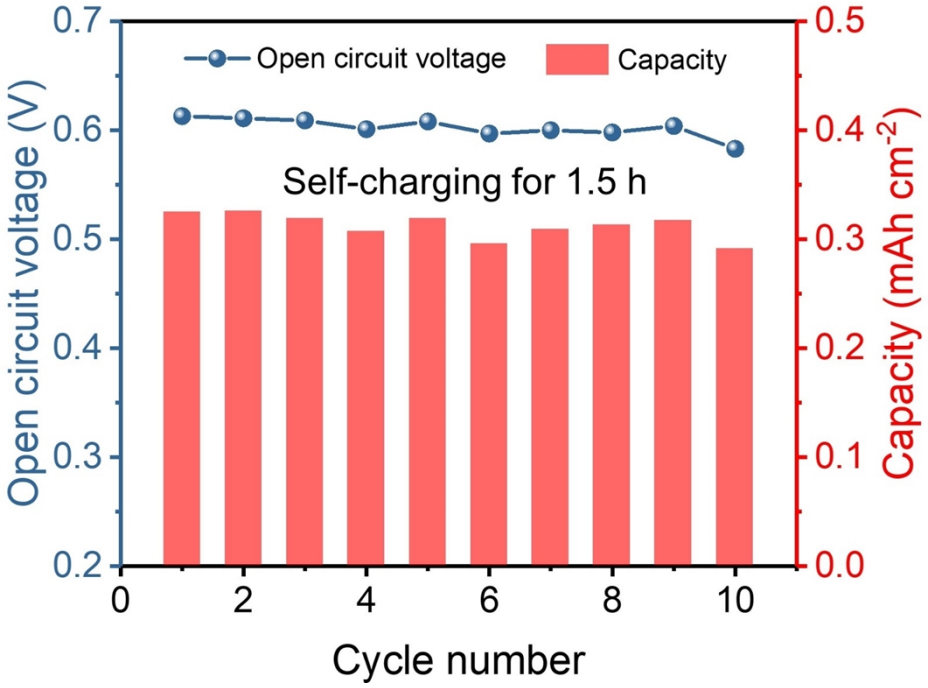

Figure S7. Effect of the cycle number on OCV and discharge capacity of the chemically self-charging I_2-H_2 batteries after self-charging for 1.5 h.

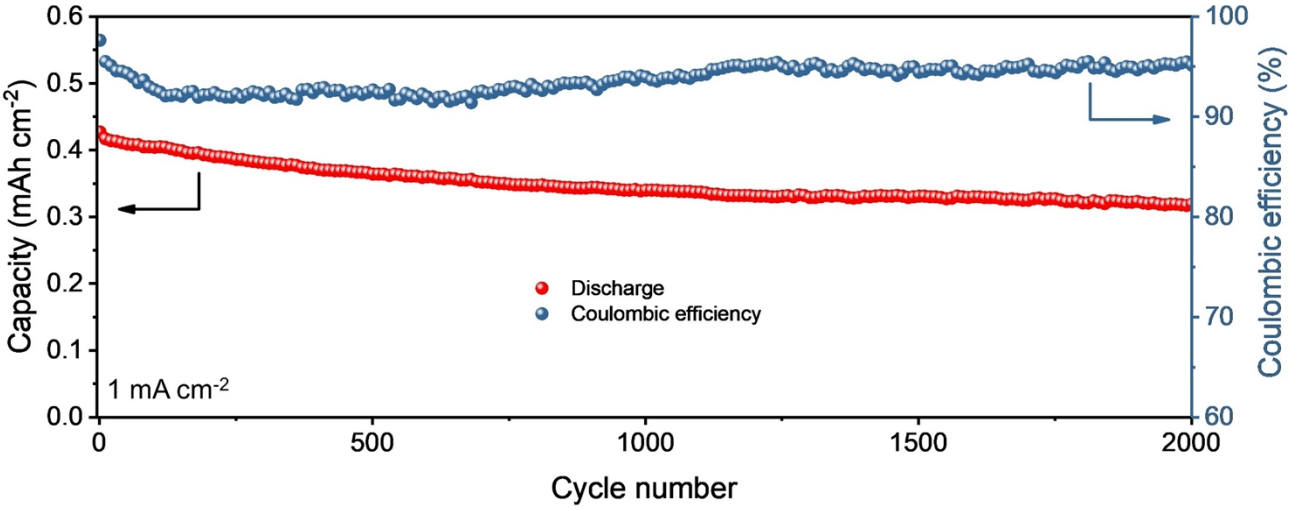

Figure S8. Cycle performance of the chemically self-charging I_2-H_2 battery at a current density of 1 mA cm^{-2} after one self-charge/discharge cycle.

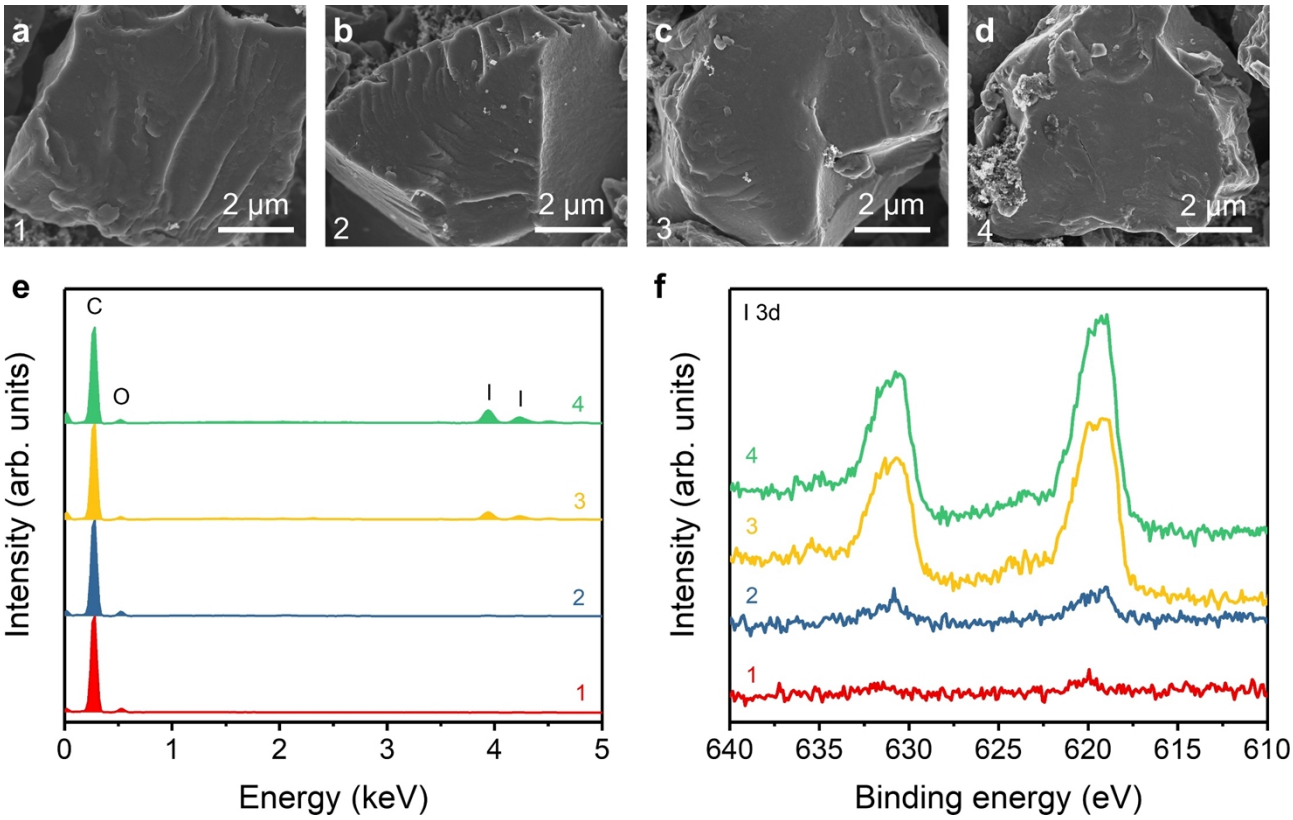

Figure S9. (a-d) SEM images, (e) EDX, and (f) XPS of I element of AC electrode in the self-charge and discharge states of the chemically self-charging I_2-H_2 batteries. State 1 is the pristine state. State 2 is the discharge state. State 3 is the self-charging state. State 4 is the power charging state.

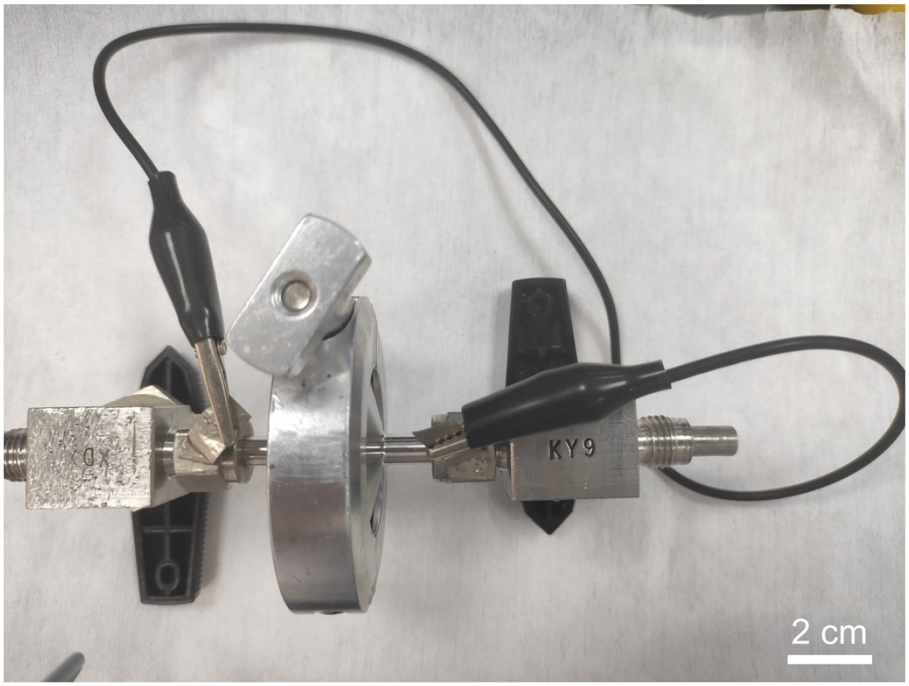

Figure S10. The external short-circuit induced setup of the short-circuit induced self-charging PBA-H_2 battery.

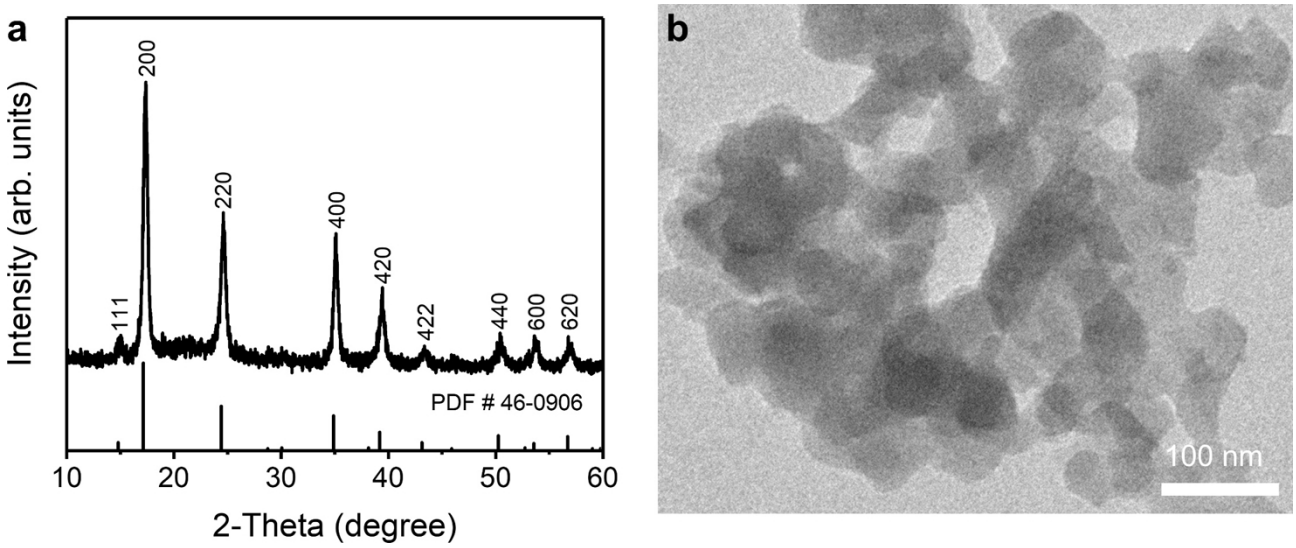

Figure S11. (a) XRD pattern and (b) TEM image of the NiHCF material.

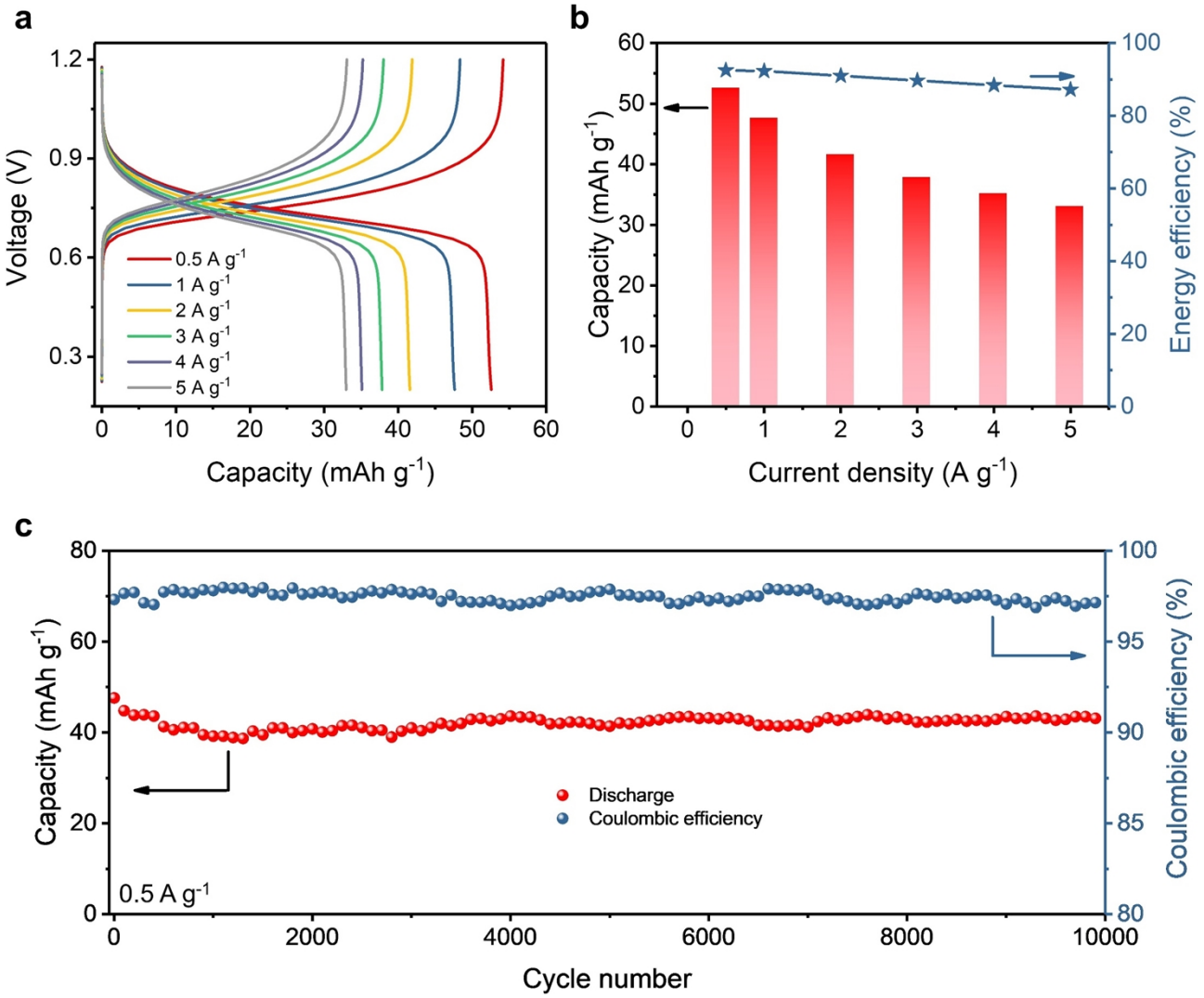

Figure S12. Electrochemical performance of PBA-H_2 batteries. (a) Rate charge/discharge curves. (b) Discharge capacity and energy efficiency at various current densities. (c) Cycle performance at a current density of 0.5 A g^{-1}.

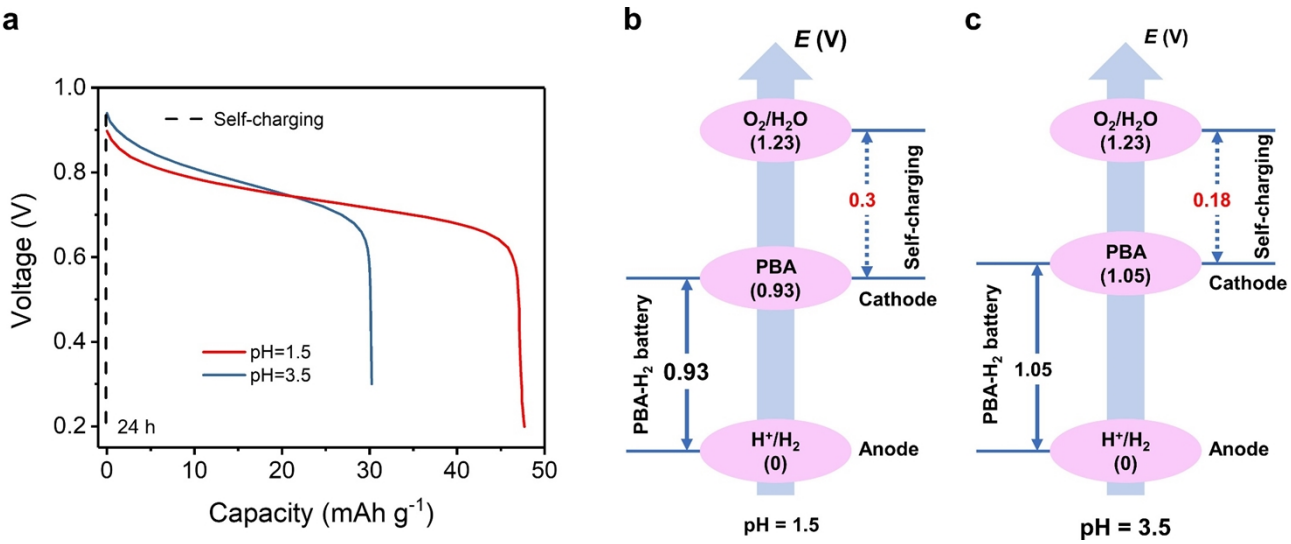

Figure S13. (a) Galvanostatic discharge curves of short-circuit induced self-charging PBA-H_2 batteries in different pH values at 0.5 A g^{-1} after self-charging for 24 h. Schematic diagram of different electrode potentials of short-circuit induced self-charging PBA-H_2 batteries in the electrolytes with (b) pH of 1.5 and (c) pH of 3.5. To compare more easily, the potentials of H_2 electrode are all set to zero and the potentials of other electrodes are relative to H_2 electrode in the schematic diagram.

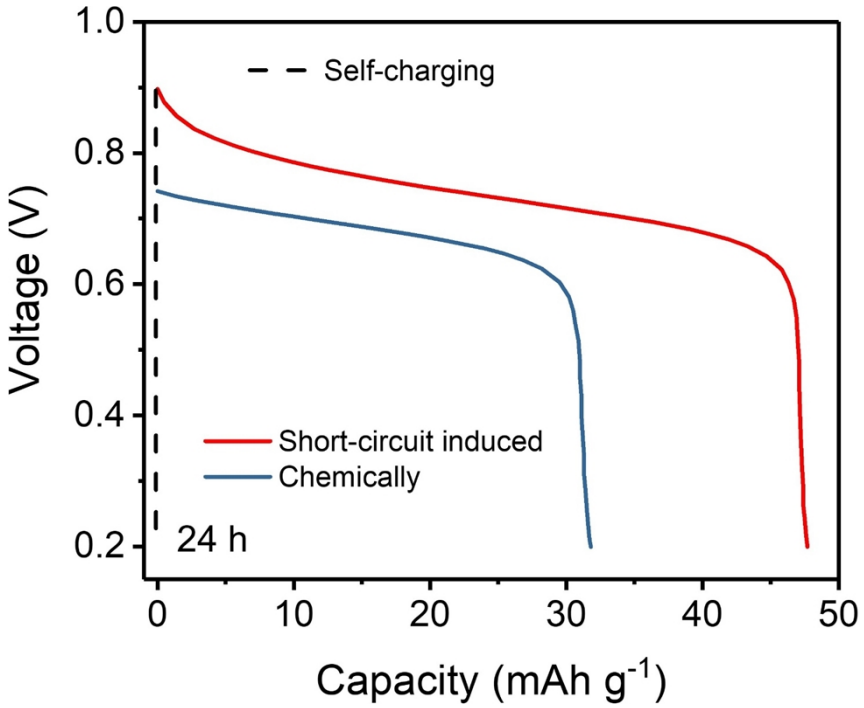

Figure S14. Galvanostatic discharge curves of chemically self-charging and short-circuit induced self-charging PBA-H_2 batteries at 0.5 A g^{-1} after self-charging for 24 h.

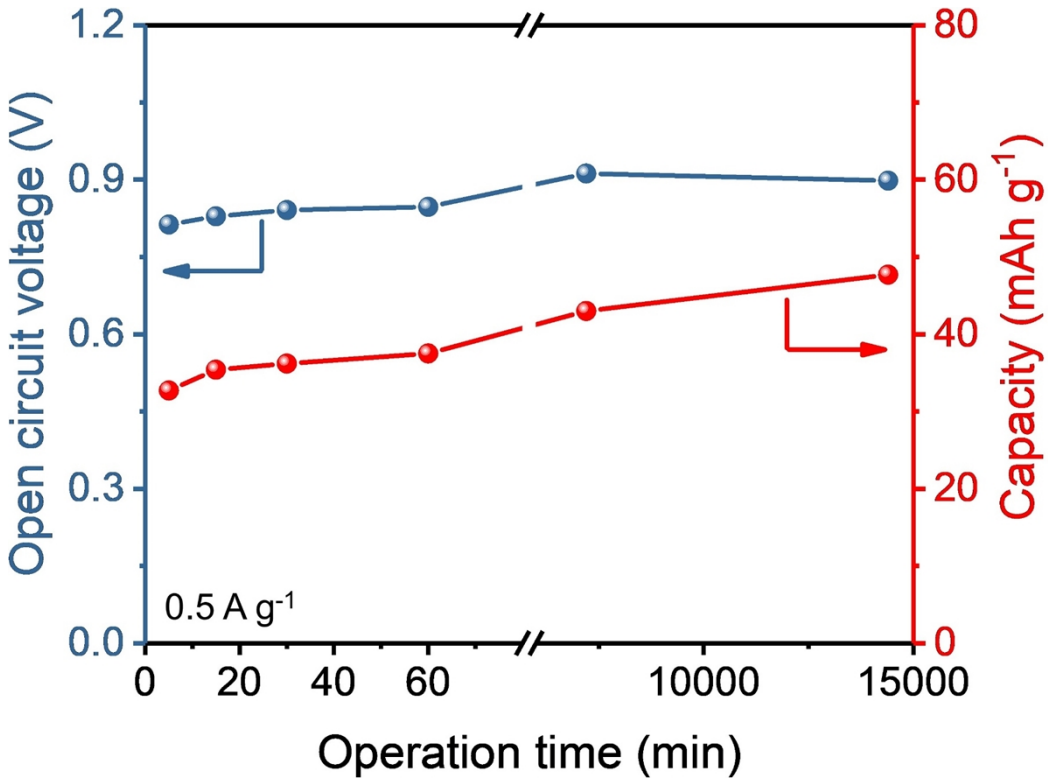

Figure S15. Effect of the self-charging time on OCV and discharge capacity of the short-circuit induced self-charging PBA-H_2 batteries.

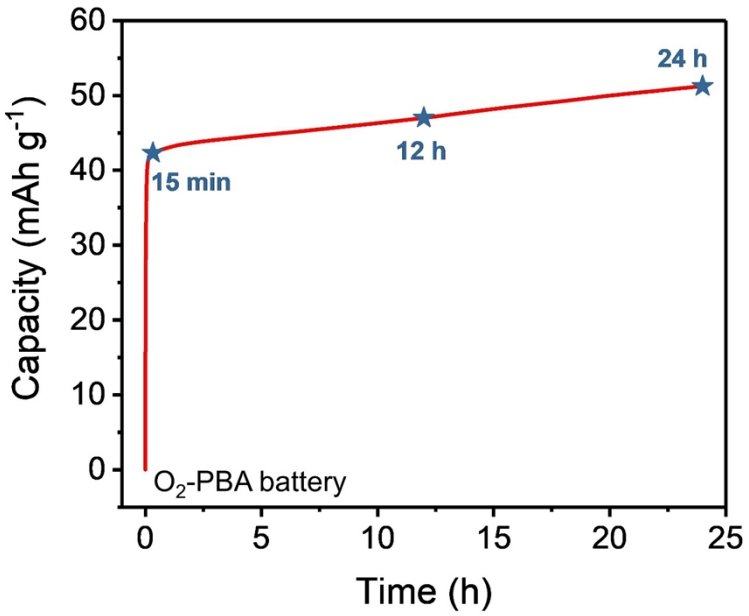

Figure S16. Charge curve of the constructed short-circuit induced O_2-PBA battery.

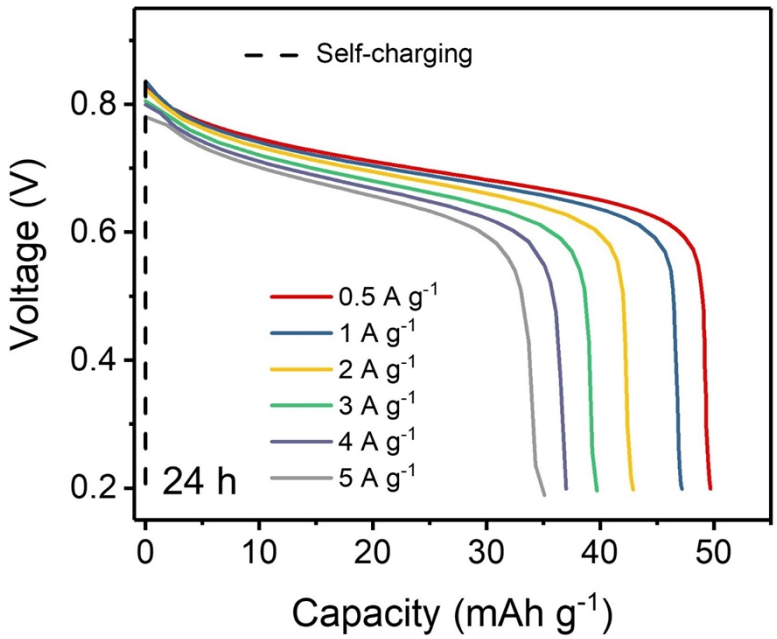

Figure S17. Rate discharge curves of the short-circuit induced self-charging PBA-H_2 batteries after self-charging for 24 h.

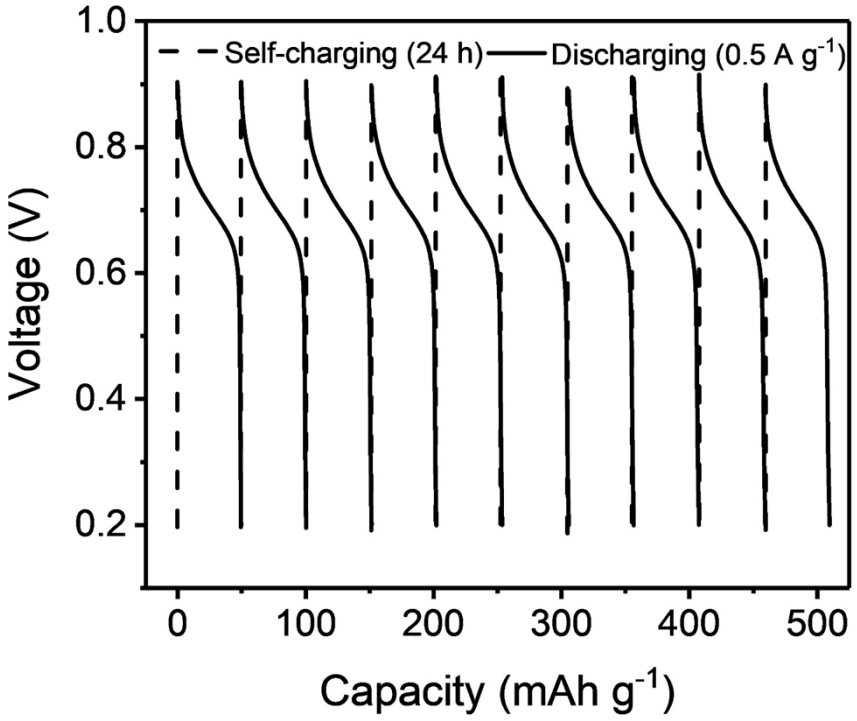

Figure S18. Repeated self-charge/galvanostatic discharge cycles of the short-circuit induced self-charging PBA-H_2 battery at 0.5 A g^{-1} after self-charging for 24 h.

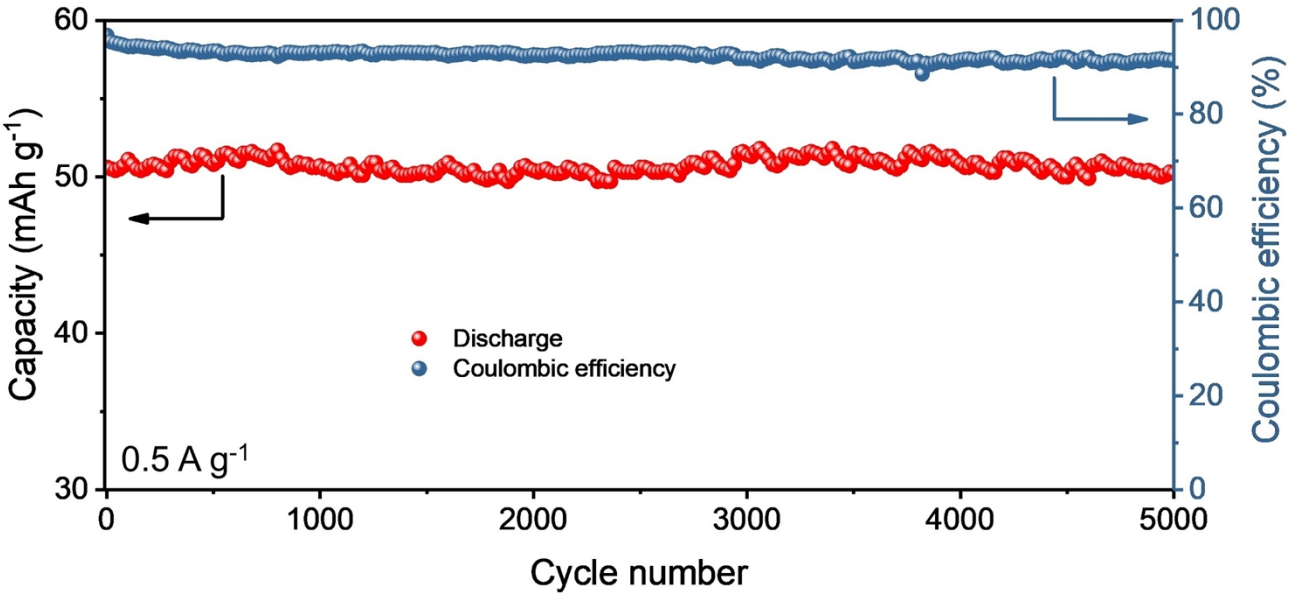

Figure S19. Cycle performance of the short-circuit induced self-charging PBA-H_2 battery at 0.5 A g^{-1} after one self-charge/discharge cycle.

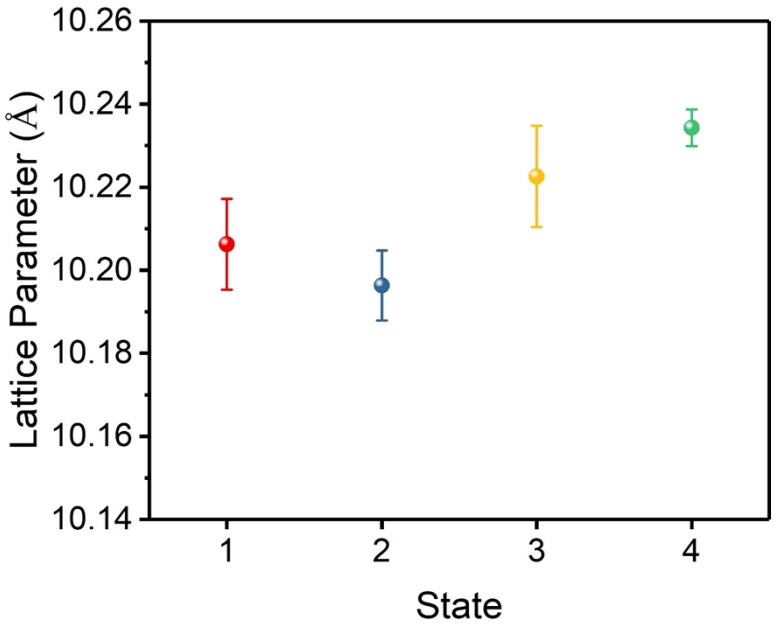

Figure S20. Changes of lattice parameter of the NiHCF materials in different charge and discharge states. State 1 is the pristine state. State 2 is the discharge state. State 3 is the self-charging state. State 4 is the power charging state. The reported lattice parameters are the average of the lattice parameters determined from diffraction peak positions of (200) and (220) planes for each sample, and the error bars in Figure S20 represent one standard deviation from the mean calculated lattice.

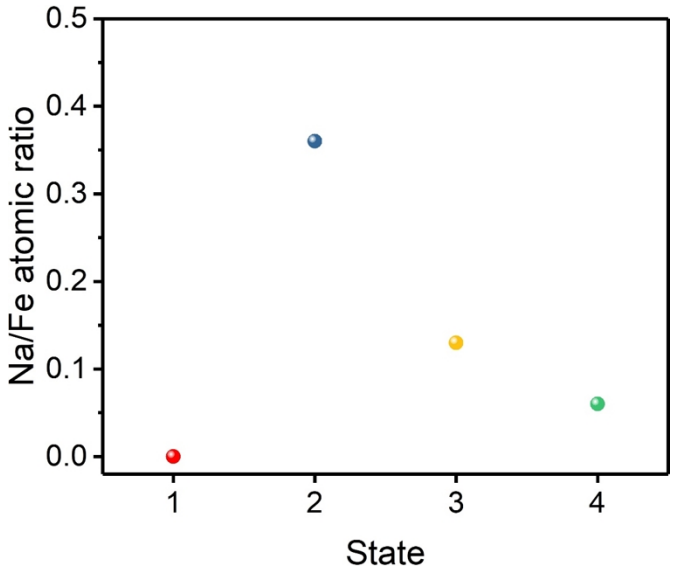

Figure S21. Surface atomic ratio of Na/Fe in the NiHCF materials in different charge and discharge states. State 1 is the pristine state. State 2 is the discharge state. State 3 is the self-charging state. State 4 is the power charging state. As shown in Figure S21, the Na/Fe ratio increases from 0 to 0.36 during the discharge, and then decreases from 0.36 to 0.13 during the self-charging and from 0.36 to 0.06 during the power charging, respectively.

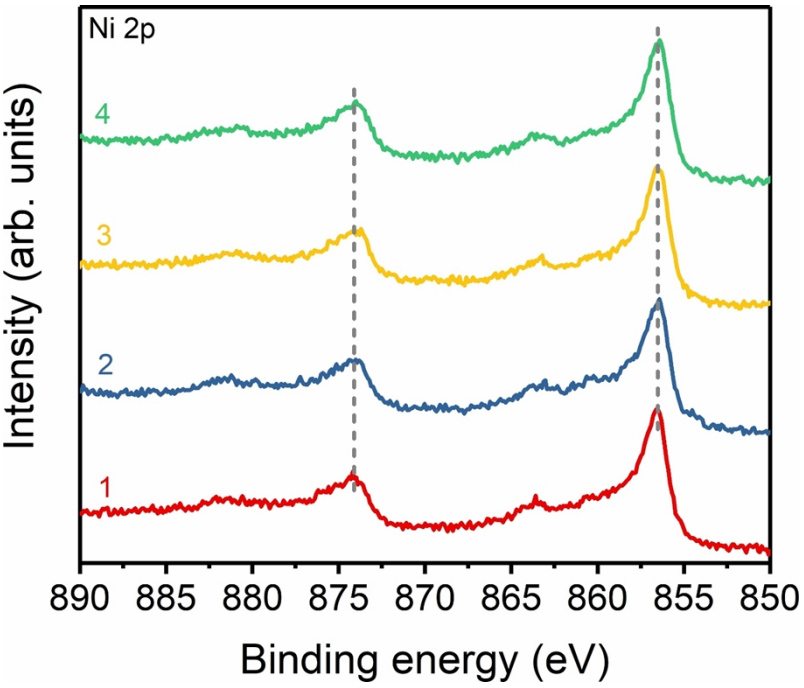

Figure S22. XPS spectra of Ni elements for the NiHCF materials in different states. State 1 is the pristine state. State 2 is the discharge state. State 3 is the self-charging state. State 4 is the power charging state.

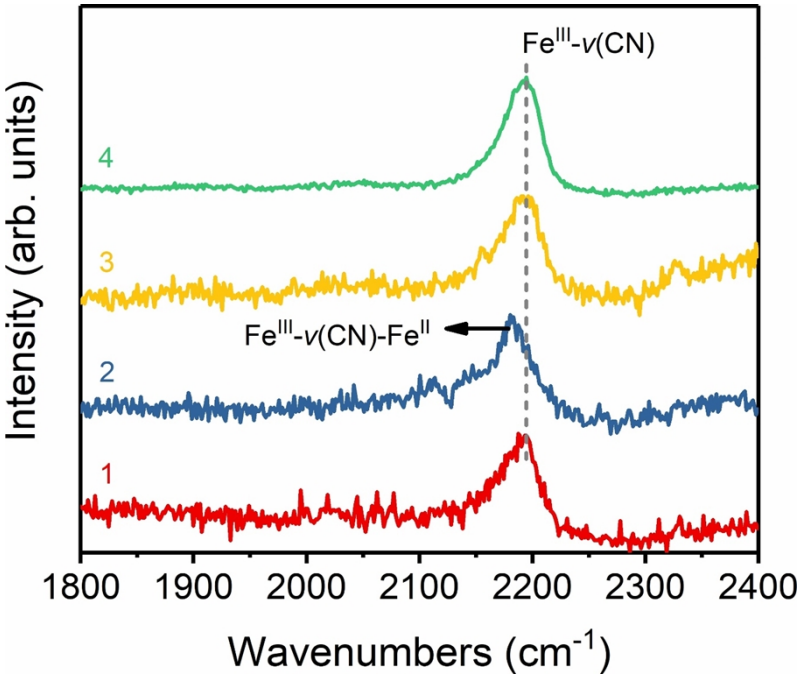

Figure S23. Raman spectra of the NiHCF materials in different states. State 1 is the pristine state. State 2 is the discharge state. State 3 is the self-charging state. State 4 is the power charging state.

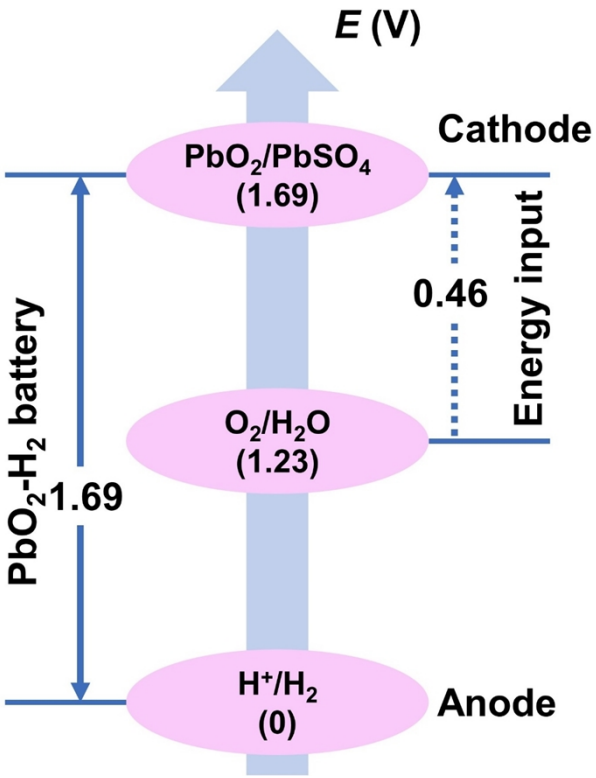

Figure S24. Schematic diagram of different electrode potentials of low-energy-input triggered quasi-self-charging PbO_2-H_2 battery.

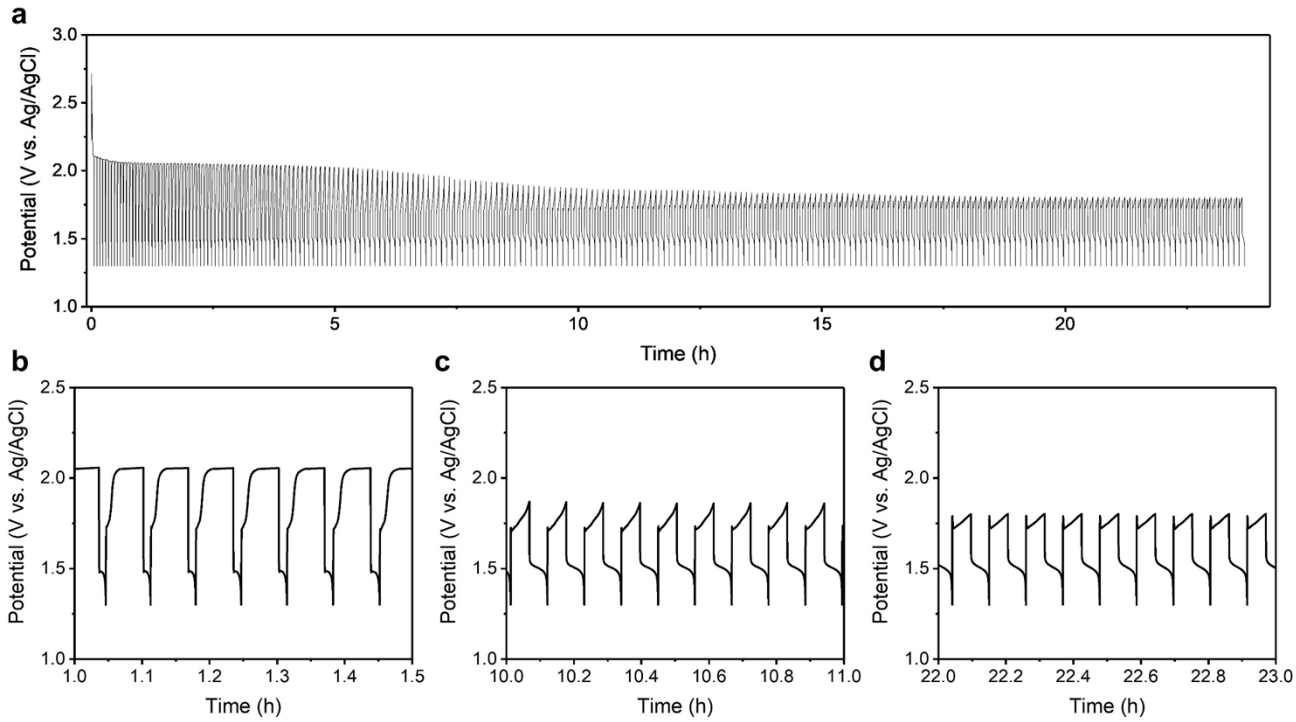

Figure S25. Galvanostatic charge/discharge curves of the breaker cell with lead foil as working electrode, platinum foil as counter electrode, and Ag/AgCl as reference electrode at a current of 60 mA with a charge time of 200 s.

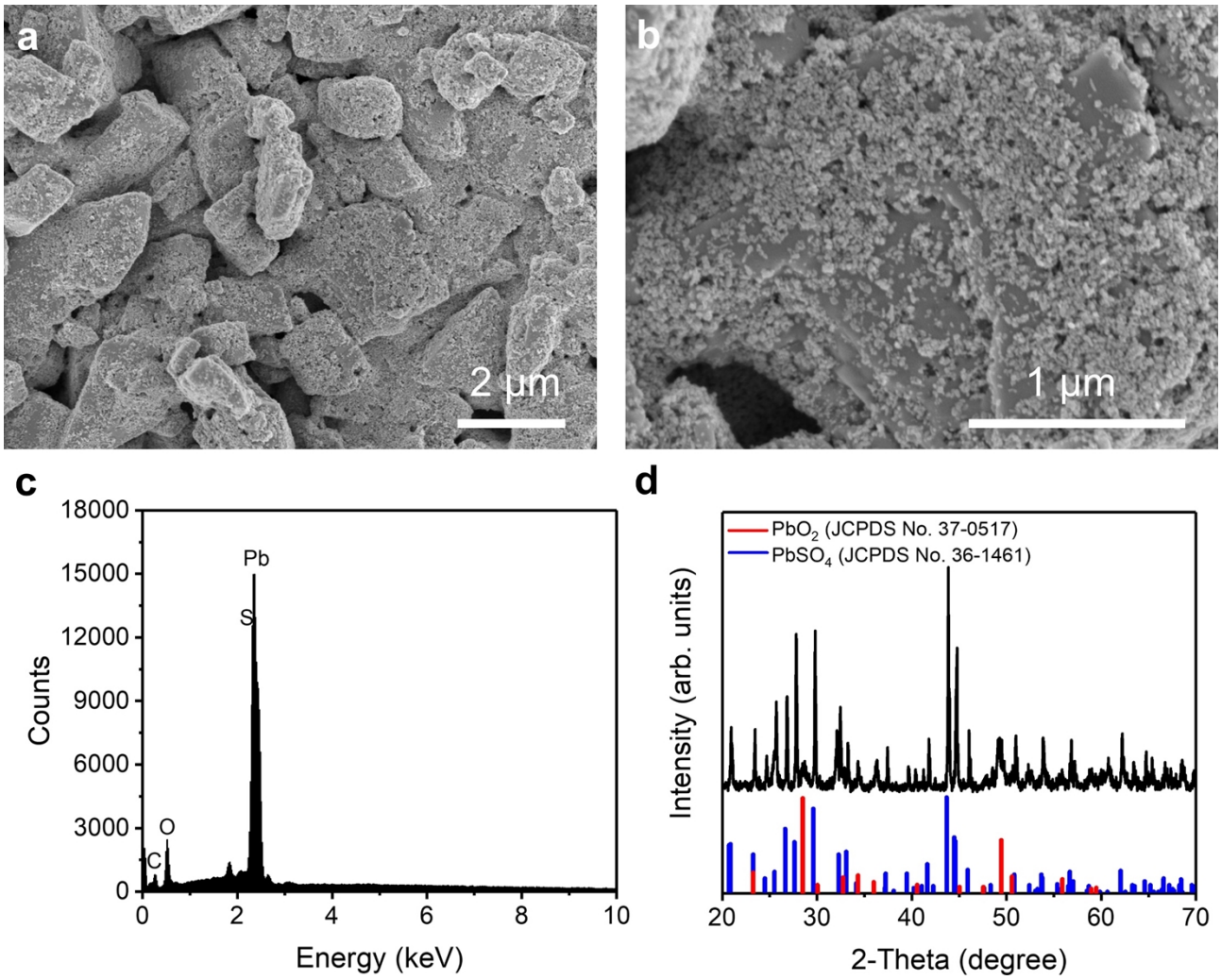

Figure S26. Characterizations of the PbO_2 material. (a, b) SEM images. (c) EDX spectra. (d) XRD pattern.

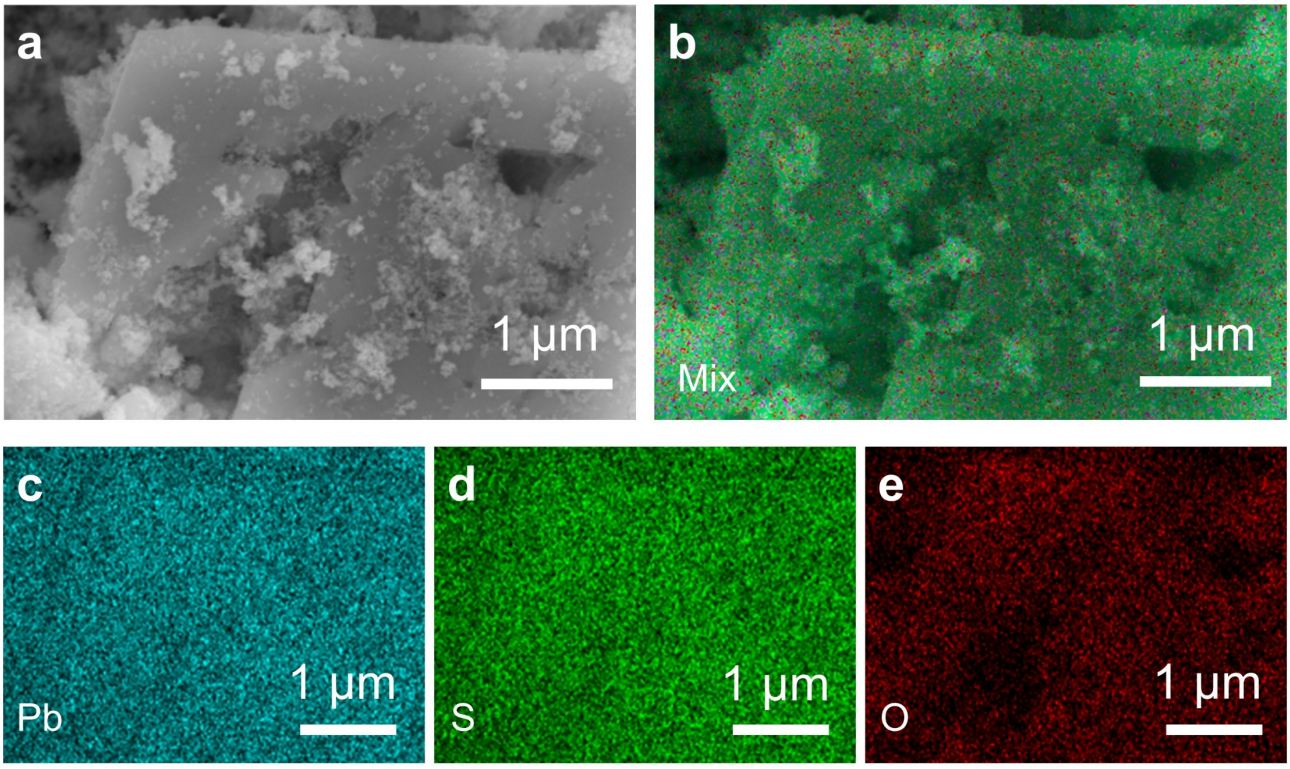

Figure S27. (a) SEM image, (b) the overlapped and (c-e) individual elemental mapping images of (c) Pb, (d) S, and (e) O of the PbO_2 cathode, respectively.

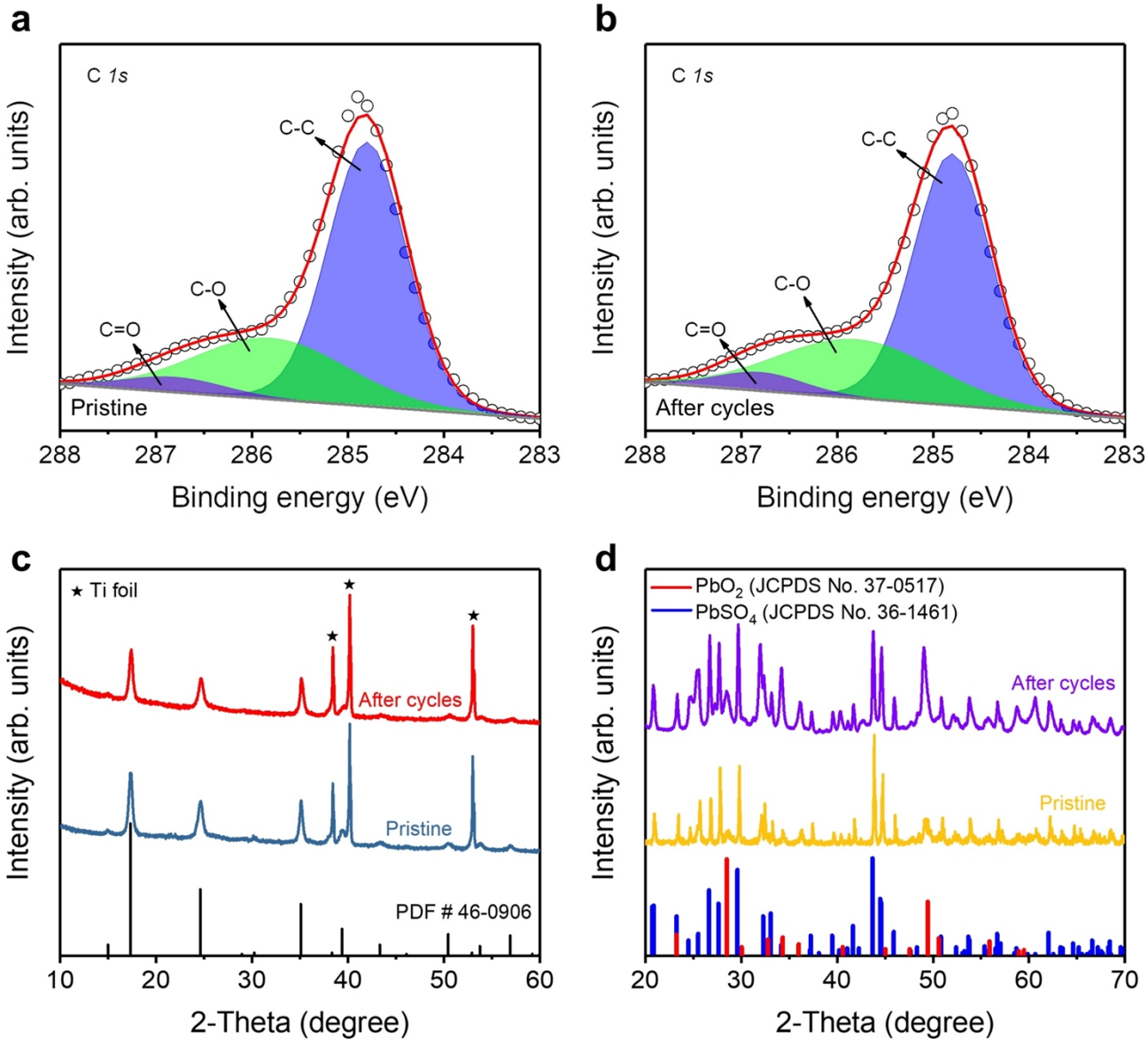

Figure S28. XPS spectra of (a) pristine AC electrode and (b) AC electrode after cycles in the chemically self-charging battery. The C 1s XPS spectra of the two AC electrodes (Figure R27a,b) exhibited three main peaks with binding energies of 286.8, 285.8 and 284.8 eV, corresponding to three functional groups of C=O, C-O and C-C, respectively. Evidently, the proportion of each functional groups show no obvious degradation after cycles. (c) XRD patterns of NiHCF electrode in the pristine state and after cycles in the short-circuit induced self-charging battery. (d) XRD patterns of PbO_2 electrode in the pristine state and after cycles in the low-energy-input triggered quasi-self-charging battery.

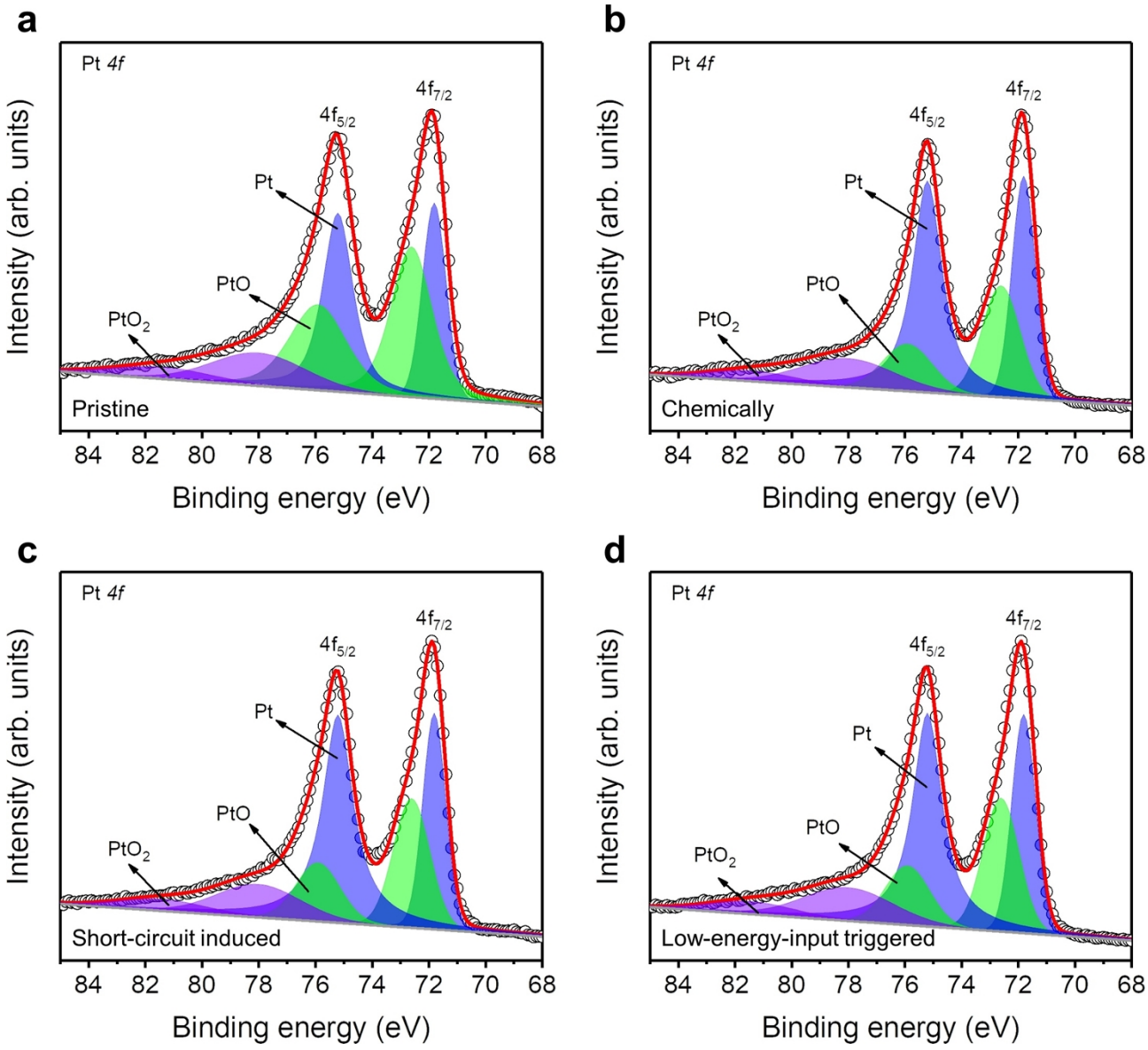

Figure S29. XPS spectra of (a) pristine Pt/C electrode, (b) Pt/C electrode after cycles in the chemically self-charging battery, (c) Pt/C electrode after cycles in the short-circuit induced self-charging battery, and (d) Pt/C electrode after cycles in the low-energy-input triggered quasi-self-charging battery. The peaks with binding energies of 71.8 and 75. 2 eV are ascribed to the $4f_{7/2}$ and $4f_{5/2}$ peaks of Pt, respectively. The peaks with higher binding energies (72.6 and 75.9 eV) are assigned to the $4f_{7/2}$ and $4f_{5/2}$ peaks of PtO, respectively. In addition, the peaks with binding energy of 78.2 eV and 82 eV correspond to the $4f_{7/2}$ and $4f_{5/2}$ peaks of PtO_2. The results prove that slight reduction is occurred to the Pt electrode in three self-charging H_2 batteries after cycles with the increase of the proportion of Pt.

Table S1 Comparison of the byproduct after cycle, cell voltage, and self-charging cycle performance of SCAHGBs with various self-charging aqueous metal-based batteries.

Type of self-charging cell	Anode	Self-charge cathode	Byproduct after cycle	Current density	Cell voltage (V)	Capacity retention /cycle number	Ref
Chemically	Al	Prussian blue	Al^{3+}/OH^-	2 A g^{-1}	1.1	~79%/3 times	5
Chemically	Zn	CaVO	Zn^{2+}/OH^-	0.1 A g^{-1}	0.7	~69%/5 times	6
Chemically	Zn	VO_2	Zn^{2+}/OH^-	0.2 A g^{-1}	~0.67	~76%/10 times	7
Chemically	Zn	PANINA	Zn^{2+}/OH^-	1 A g^{-1}	~1	~90%/3 times	8
Chemically	Zn	BQPH	Zn^{2+}/OH^-	0.1 A g^{-1}	0.77	~68%/4 times	9
Chemically	Zn	Poly(1,5-NAPD)	Zn^{2+}/OH^-	0.2 A g^{-1}	~0.74	~91%/10 times	10
Chemically	Pb	PTO	$PbSO_4/OH^-$	0.2 A g^{-1}	0.72	~89%/10 times	11
Chemically	**H_2**	**I_2**	**H^+/OH^-**	**1 mA cm^{-2}**	**0.46**	**~90%/10 times**	**This work**
Short-circuit induced	**H_2**	**PBA**	**H^+/OH^-**	**0.5 A g^{-1}**	**0.74**	**~97%/10 times**	**This work**
Low-energy-input triggered	**H_2**	**PbO_2**	**H^+/OH^-**	**20 mA cm^{-2}**	**1.69**	**~100%/10 times**	**This work**

Table S2. The advantages and shortcomings of three self-charging battery systems.

	Advantage	Shortcoming
Chemically	High cycle stability, wide application range in H_2 batteries and other metal-based batteries, no extra energy input, self-charging system	Low working voltage, low energy output, slow self-charging rate
Short-circuit induce	High cycle stability, fast self-charging rate, no extra energy input, self-charging system	Low working voltage, low energy output
Low-energy-input triggered	High cycle stability, fast self-charging rate, high working voltage, high energy output	Need energy input, pseudo self-charging system

References

(1) Zhu, Z.; Meng, Y.; Yin, Y.; Liu, Z.; Jiang, T.; Peng, Q.; Yin, T.; Li, M.; Chen, W. High performance aqueous Prussian blue analogue-hydrogen gas hybrid batteries. *Energy Storage Mater.* **2021**, *42*, 464-469.

(2) Zhu, Z.; Liu, Z.; Yin, Y.; Yuan, Y.; Meng, Y.; Jiang, T.; Peng, Q.; Wang, W.; Chen, W. Production of a hybrid capacitive storage device via hydrogen gas and carbon electrodes coupling. *Nat. Commun.* **2022**, *13*, 2805.

(3) Zhu, Z.; Meng, Y.; Wang, M.; Yin, Y.; Chen, W. A high-performance aqueous iron–hydrogen gas battery. *Mater. Today Energy* **2021**, *19*, 100603.

(4) Zhu, Z.; Wang, W.; Yin, Y.; Meng, Y.; Liu, Z.; Jiang, T.; Peng, Q.; Sun, J.; Chen, W. An Ultrafast and Ultra-Low-Temperature Hydrogen Gas-Proton Battery. *J. Am. Chem. Soc.* **2021**, *143*, 20302-20308.

(5) Wang, J.; Zhang, L.; Yu, L.; Jiao, Z.; Xie, H.; Lou, X. W.; Sun, X. W. A bi-functional device for self-powered electrochromic window and self-rechargeable transparent battery applications. *Nat. Commun.* 2014, 5, 4921.

(6) Zhang, Y.; Wan, F.; Huang, S.; Wang, S.; Niu, Z.; Chen, J. A chemically self-charging aqueous zinc-ion battery. *Nat. Commun.* **2020**, 11, 2199.

(7) Liu, C.; Xu, W.; Mei, C.; Li, M.; Chen, W.; Hong, S.; Kim, W. Y.; Lee, S. y.; Wu, Q. A Chemically Self-Charging Flexible Solid-State Zinc-Ion Battery Based on VO_2 Cathode and Polyacrylamide–Chitin Nanofiber Hydrogel Electrolyte. *Adv. Energy Mater.* **2021**, 11, 2003902.

(8) Xie, X.; Fang, Z.; Yang, M.; Zhu, F.; Yu, D. Harvesting Air and Light Energy via "All-in-One" Polymer Cathodes for High-Capacity, Self-Chargeable, and Multimode-Switching Zinc Batteries. *Adv. Funct. Mater.* **2021**, 31, 2007942.

(9) Tie, Z.; Zhang, Y.; Zhu, J.; Bi, S.; Niu, Z. An Air-Rechargeable Zn/Organic Battery with Proton Storage. *J. Am. Chem. Soc.* **2022**, 144, 10301-10308.

(10) Yan, L.; Zhang, Y.; Ni, Z.; Zhang, Y.; Xu, J.; Kong, T.; Huang, J.; Li, W.; Ma, J.; Wang, Y. Chemically Self-Charging Aqueous Zinc-Organic Battery. *J. Am. Chem. Soc.* **2021**, 143, 15369-15377.

(11) Yue, F.; Tie, Z.; Zhang, Y.; Bi, S.; Wang, Y.; Niu, Z. Proton Chemistry Induced Long-Cycle Air Self-Charging Aqueous Batteries. *Angew. Chem. Int. Ed.* **2022**, 61, e202208513.